Computers and Geotechnics 154 (2023) 105118

Contents lists available at ScienceDirect

Computers and Geotechnics

journal homepage: www.elsevier.com/locate/compgeo

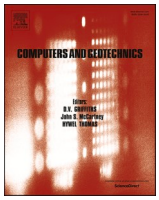

A multi-field and fluid–solid coupling method for porous media based on DEM-PNM

Yao Zhu [a], Chun Liu [a,b,*], Hui Liu [a], Yu-dong Kou [a], Bin Shi [a]

[a] School of Earth Sciences and Engineering, Nanjing University, Nanjing, China
[b] State Key Laboratory for GeoMechanics and Deep Underground Engineering, China University of Mining & Technology, Beijing, China

ARTICLE INFO

Keywords:
Discrete element method
Pore network model
Multi-field coupling
Fluid-solid coupling
MatDEM

ABSTRACT

Many processes in geology and geotechnical engineering fields involve multi-field coupling, fluid–solid coupling and large deformation. The numerical simulation of such complicated processes is still very challenging. Based on the Discrete Element Method, a pore density flow model is proposed to simulate multi-field coupling and fluid–solid coupling, which introduces the Pore Network Model to describe the pores. The fluid properties within a single pore are normalized to reduce the computational complexity and determine the amount of fluid exchange based on the Darcy's Law. Moreover, an equation including density, pressure and temperature is introduced to simulate fluid state. The pore network changes dynamically with the displacement of elements, which can simulate the cracking and failure process of complex rock and soil mass driven by fluids. This model is implemented in the high-performance discrete element software MatDEM, which can quantitatively analyze the evolution law of fluid–solid coupling in the pore scale. Three examples are given to verify the validity of this model. The simulation results show that this model can not only form an effective network model based on the DEM, but also can reflect the immigration of fluids and heat in the porous medium and the development trend of fluid-driven fractures.

1. Introduction

A large number of geotechnical engineering problems involve fluid–solid coupling, multi-field coupling and large deformation, such as rainfall-induced landslides, water and mud inrush in tunnels, and freeze–thaw cycles of frozen soil (Long et al., 2022; Liu et al., 2020; Zhou et al., 2021b). However, numerical simulation and analysis of complex engineering geological problems that involve multi-field coupling and large deformation are still very challenging. On the macroscopic scale, the rock and soil mass can be considered as a continuous medium, and problems such as seepage and multi-field coupling can be simulated by methods such as finite element and finite difference (Huang and Jia, 2009; Qu et al., 2020). However, on the microscopic scale, the rock and soil mass are composed of solids, pores and fluids in the pores, which constitutes the problem of fluid–solid coupling (Kuhn and Daouadji, 2020). Regular continuum mechanics methods, such as the Finite Element Method, has been widely applied in the analysis of multi-field coupling processes. However, they still have difficulties in numerical simulations of large deformations and failures of medium. In the Discrete Element Method (DEM) (Cundall and Strack, 1979), rock and soil blocks are represented by a series of cemented elements. Large deformation failure processes, such as the evolution of landslides (Lu et al., 2014) and the liquefaction of sands (Sizkow and El Shamy, 2022), can be well simulated in this method.

The fluid–solid coupling method based on DEM is the focus of current research. At present, the common methods for coupled calculation with DEM are Computational Fluid Dynamics (CFD) (Zhou et al., 2019; Norouzi et al., 2016), Smoothed Particle Hydrodynamics (SPH) (Sizkow and El Shamy, 2021; Xu et al., 2020) and Lattice Boltzmann Method (LBM) (Han and Cundall, 2013; Huang et al.2021). Both DEM-CFD and DEM-SPH are solved by the Navier–Stokes (N-S) equation. DEM-CFD usually adopts the incomplete solution method. In this method, the computing grid size of fluid is larger than the diameter of solid elements, which is suitable for large-scale macroscopic 3D fluid–solid coupling numerical simulation (Zhou et al., 2019), such as landslide surge simulation (Nian et al., 2021). DEM-SPH describes continuous fluids (or solids) as groups of interacting elements. This method has advantages in the fluid–solid coupling simulation of fluids with free surfaces. In this method, the resolution of the fluid needs to be at least twice that of the solid element size, which lacks stability and accuracy. Both DEM-CFD and DEM-SPH have difficulties in numerical simulation in the pore scale (Zheng et al., 2010). A lattice Boltzmann formulation of the

* Corresponding author.

https://doi.org/10.1016/j.compgeo.2022.105118
Received 4 August 2022; Received in revised form 30 September 2022; Accepted 27 October 2022
Available online 30 November 2022

generalized Navier-Stokes equations is used to describe the fluid motion in the DEM-LBM. In this method, discrete element elements are regarded as a moving object in the fluid, and their shape and size are described by the LBM lattice (Rettinger and Rüde, 2018). The mesh size of this method is one order of magnitude smaller than that of solid elements, so this method can better simulate the coupling between elements and the surrounding fluid. At present, this method has been applied in the liquefaction of sands (Indraratna et al., 2021), porous media fluids (Zhou et al., 2021a) and other problems. The DEM-LBM can accurately simulate complex multi-field, multiphase and multiscale problems. However, this method requires a large amount of calculation. In the three-dimensional case, the simulation scale of the DEM-LBM is usually limited to hundreds of elements (Han and Cundall, 2013), which limits its application at the engineering scale.

In recent years, the French open source software Yade team began to develop numerical simulations of fluid–solid coupling based on the Pore Network Model (PNM) (Catalano et al., 2013) to meet the needs of large-scale fluid–solid coupling. The intermediate scale introduced by the PNM discretizes the pore space into a set of fluid domains and pore throats. This method does not need to solve the N-S equations, which effectively improves the calculation efficiency. At present, DEM-PNM has been applied in many fields, such as fluid flows between particles (Wautier et al., 2017), granular material drying (Kharaghani et al., 2011) and drainage in granular materials (Yuan et al., 2016). However, in this model, the fluid state equation is generally solved by the bulk modulus, which cannot effectively consider the effect of temperature and density on the fluid state. Moreover, the redivision of network caused by the displacement of solid elements also has some shortcomings, so it is usually limited to static or quasi-static problems such as seepage.

This paper constructs a pore density flow model that includes the seepage model, the hydrothermal coupling model and the fluid–solid coupling model for overcoming the shortcomings of the above model. In this model, a fluid state equation containing temperature, density and pressure is introduced to consider the effect of temperature on seepage calculations, which can be used to ensure the correctness of the pore seepage calculation under non-isothermal action. In addition, the dynamic identification of the pore network structure and state is achieved during the deformation and failure of solids that considers the process of merging and splitting of pores and fractures for solving the problem of fluid-driven failure in porous media.

This paper is organized as follows. First, a pore seepage model is presented, which considers the structure of pores based on the discrete element packing model. The equations of fluid state and thermal exchange are applied to establish a hydrothermal coupling model based on the seepage model. Then the dynamic division of the pore network is applied to the fluid–solid coupling model. Finally, the pore density flow model is thoroughly verified through three numerical examples. A geothermal model tank experiment and a hydraulic fracturing experiment are simulated using the hydrothermal coupling model and fluid–solid coupling model to study the laws of geothermal transmission and the developmental trends in fracture driven by fluid.

2. The basic principle of DEM

In the DEM, rock and soil mass are modeled by stacking elements with specific mechanical properties. The macroscopic mechanical properties of the model are affected by the properties of the elements, the packing process, and the cementation. In the linear elastic model, it is assumed that the elements rely on springs to contact each other and generate force (Jiang et al., 2012; Liu et al., 2013; Liu et al., 2015). The normal force and normal deformation between elements can be simulated by normal springs between elements (Place and Mora, 1999):

$$F_n = \begin{cases} K_n X_n, & X_n < X_b \quad Completeconnectiona \\ K_n X_n, & X_n < 0 \quad Brokenconnectionb \\ 0, & X_n > 0 \quad Brokenconnectionc \end{cases} \tag{1}$$

where K_n is the normal stiffness of the spring, X_n is the normal relative displacement (Fig. 1a), and X_b is the fracture displacement. Initially, elements are interconnected with their adjacent elements and subjected to tensile or compressive spring forces (Eq. 1a and Eq. (1b)). When X_n between the two elements exceeds the fracture displacement (X_b), the spring breaks and the interelement tensile force no longer exists between them (Eq. (1c)); However, the compressive force may act between them when they return to a compressive status.

The shear force (F_s) and shear deformation (X_s) between elements are simulated by tangential springs (Place and Mora, 1999):

$$F_s = K_s X_s \tag{2}$$

where K_s is the shear stiffness and X_s is the shear relative displacement.

The spring also has a failure criterion in the tangential direction, which is based on the Mohr–Coulomb criterion:

$$F_{\mathrm{smax}} = F_{\mathrm{s0}} - \mu_p F_n \tag{3}$$

where F_{smax} is the maximum shear force, $F_{s0\ is}$ the interelement initial shear resistance, and μ_p is the interelement coefficient of friction. In the Mohr–Coulomb criterion, the maximum shear resistance between elements is related to the initial shear resistance (F_{s0}). F_{s0} is the maximum shear force allowed between elements without applying normal pressure. When the magnitude of the shear force exceeds the maximum shear force determined by Eq. (2), the tangential connection is broken, and only the sliding friction force ($-\mu_p F_n$) exists between the elements.

3. The pore density flow model

Based on the DEM, the pore density flow model (PDF) introduces the pore network model to describe the pores among discrete elements. This model includes seepage models, hydrothermal coupled models, and fluid–solid coupled models, which can be used to simulate seepage and fluid-driven failure problems in saturated porous media.

The basic idea of PDF is as follows: (1) identify pores (fluid domains) and pore throats in discrete element models; (2) the fluid in the pore migrates between the pores through the pore throat, and the seepage is determined by factors such as rock and soil properties, fluid pressure difference and external load; (3) the water pressure is determined according to the temperature and density of the fluid in the pores; (4) the elements are displaced under the pressure of the fluid, which realizes the fluid–solid coupling. In this method, the pressure of the fluid can be obtained from the density and temperature. This improved method can further consider the effect of temperature on the fluid–solid coupling process during fluid migration. At the same time, we also improved the identification method of the pore network in the process of fluid–solid coupling, which can better simulate the large deformation and failure of rock and soil.

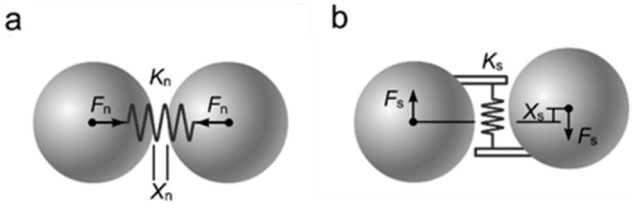

Fig. 1. Schematic diagram of the linear elastic model.

3.1. The structure of pore network based on DEM

The classic pore network model (PNM) is often considered in the Discrete Element Method (DEM) to simulate the fluid flow and fluid–solid coupling in the pore scale. The PNM is generally composed of pores and pore-throat channels with a certain transmission capacity between the pores (FATT, 1956). This method mainly studies the transfer and diffusion of fluids in a fixed network without considering the coupling between elements and pores. The advantage of this method is that the calculation speed is fast, which has been widely used in fluid–solid coupling problems in the pore scale.

Essentially, LBM simulates the migration of fluids with a certain density between networks. The macroscopic parameters of the fluid, such as the fluid pressure, are related to density. Based on the theory of DEM-PNM and the basic idea of LBM, the pore density flow model is proposed in this paper to simulate fluid–solid coupling. In this model, rocks and soils are discretized into elements (Fig. 2a), and the voids between elements are defined as pores (Fig. 2b, See Fig. 3 for details). The pores are filled with fluids with the same physical properties. Pore throats are defined as channels connecting pores, which are gaps between elements in a discrete element system. In this model, pore throats with a certain width and length are used to control fluid transport. Pores and pore throats make up the pore network model (Fig. 2 c).

As shown in Fig. 3, in case of a two-dimensional model, we abstract the pore throat (the dashed rectangle in Fig. 3) as a parallel plate with a certain thickness and length. In the three-dimensional model, it is abstracted as a cylinder with a certain length. When there is a pressure difference between two adjacent pores, the fluid will seep through the pore throat channel which can be calculated by Darcy's law. In this paper, the flow rate (q) through the pore throat per unit time is defined as:

$$q = kA\frac{dP}{l} \tag{4}$$

where k represents the permeability coefficient of the pore throat, which is inversely proportional to the length of the pore throat and proportional to the width; dP is the pressure difference between adjacent pores. A is the area of the pore throat, which is equal to the width d_w of the pore throat in a two-dimensional problem. The length l of the pore throat is defined as:

$$l = min(R_1, R_2) \tag{5}$$

The distance between the centers of the two elements with radii R_1 and R_2 is L. In the Discrete Element Method, the distance between the elements is used to determine whether the elements are in contact, which is used to determine the presence of pore throats in this model. When the distance L between the elements is less than the threshold D_{max}, there is a pore throat channel between the two elements.

Generally, to reproduce the sedimentation process of rock and soil, discrete elements will be packed under gravity deposition during the modelling process. In the DEM, the elements overlap each other under the action of gravity and external loads. In this case, the pore throats are given a certain initial width to avoid unrealistic permeability coefficients ($k < 0$). Therefore the radii of the elements needs to be reduced when performing pore identification. The reduced radius is called the hydraulic radius R_w, which is defined as the product of the radius of the elements composing the pore throat and the hydraulic radius coefficient a. Therefore, the real pore throat width $d_w = L - a(R_1 + R_2)$. As shown in Fig. 3, the orange circles represent real discrete element elements, and the blue circles represent elements with hydraulic radii.

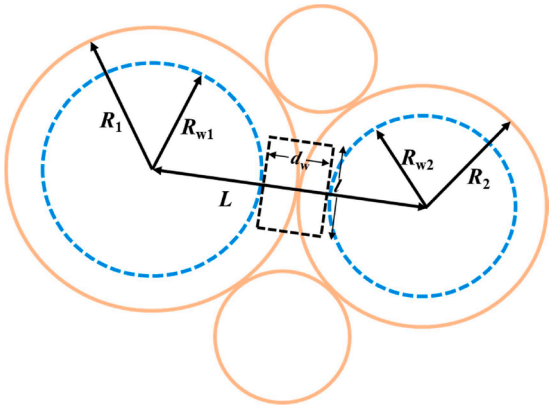

Fig. 3. Schematic diagram of the hydraulic radius (the orange circles represent real discrete element elements, and the blue dashed circles represent elements with hydraulic radii. The dashed rectangle between the two elements is the pore throat with length l and width d_w).

The permeability coefficient of pore throats is macroscopically expressed as the permeability coefficient of rock and soil. The volumetric flow rate of the model obeys the cubic law, and the flow rate of liquid through the pore throat per unit time is (Tsang and Witherspoon, 1981):

$$Q = \frac{{d_w}^3}{12\mu}\frac{dP}{l} \tag{6}$$

where μ is the dynamic viscosity of the liquid. When the solid of the accumulation model remains unchanged, the larger the permeability coefficient of the pore throat is, the larger the macroscopic permeability coefficient of the rock–soil mass. The microscopic permeability coefficient of pore throats $k = {d_w}^2/12\mu$.

The rock exhibits different permeability coefficient values in different directions, which is called the anisotropy of rock permeability coefficient. Based on Eq. (4), the anisotropy of permeability coefficient is mainly achieved by changing the microscopic permeability coefficient k. For example, we can set the microscopic permeability coefficient k to a variable k (x, y, z) which changes with the spatial position, so that the permeability coefficient in different directions can be controlled artificially.

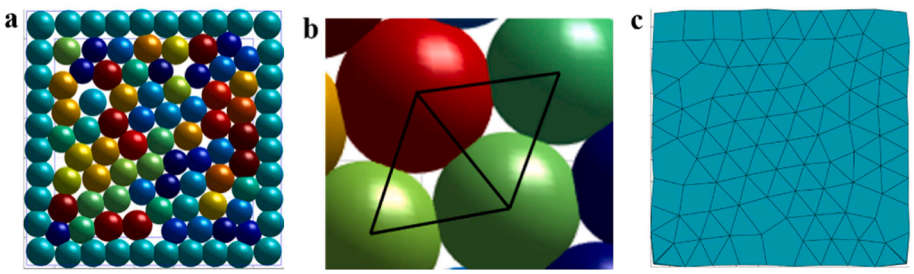

Fig. 2. (a) The basic geotechnical solid consists of discrete elements; (b) pore throats are constructed between adjacent elements, which constitute pores; (c) the pore network based on Discrete Element Model.

3.2. Fluid state equation

Most fluid–solid coupling simulations are only performed under isothermal condition, in which the bulk modulus of the fluid does not change. For problems such as geothermal activity, temperature is one of the important parameters. The bulk modulus of the fluid is greatly affected by temperature. The equation of state, which can be obtained from experimental data, can be used to quantitatively describe the fluid state. Therefore, in the pore density flow model, we introduce the variable temperature (T) into the fluid state equation. The general fluid state equation can be written as:

$$P = f(\rho, T) \tag{7}$$

By fitting the relationship between water density and temperature and pressure under saturated vapor pressure, the equation of state of water is obtained. The form of the equation is:

$$P = \frac{\rho - 999.9 - 0.03769T + 0.006417T^2 - 1.901 \times 10^{-5}T^3}{4.913 \times 10^{-7} - 2.313 \times 10^{-9}T + 2.302 \times 10^{-11}T^2} \tag{8}$$

The unit of temperature T is °C, the unit of density ρ is kg/m^3, and the unit of pressure P is MPa. When we simulate an isothermal process (taking 20 °C as an example), the equation simplifies to:

$$P = \frac{\rho - 999.75}{4.615 \times 10^{-7}} \tag{9}$$

3.3. Two-dimensional pore seepage model

When there is a pressure difference between two adjacent pores, the fluid seeps through the pore throat channel. The algebraic sum of the mass difference between the output and input of the fluid flowing through a single pore and its internal mass change is zero. Fig. 4 shows the direction of fluid movement between the fluid domain $Pore_0$ and its surrounding fluid domains $Pore_i$ ($i = 1, 2, 3\ldots$). This migration follows Darcy's law, and the fluid will spontaneously migrate from high-pressure pores to low-pressure pores. The flow rate (Q_{ij}) through the pore throat in one time step is defined as:

$$Q_{ij} = k_{ij}\frac{A_{ij}}{l_{ij}}(P_i - P_j) \tag{10}$$

where k_{ij} is the permeability coefficient of the pore throat, A_{ij} is the area of the pore throat, l_{ij} is the length of the pore throat. Fluid inflow is defined as a positive value in Eq.10.

The new mass of the fluid domain calculated after a time step is:

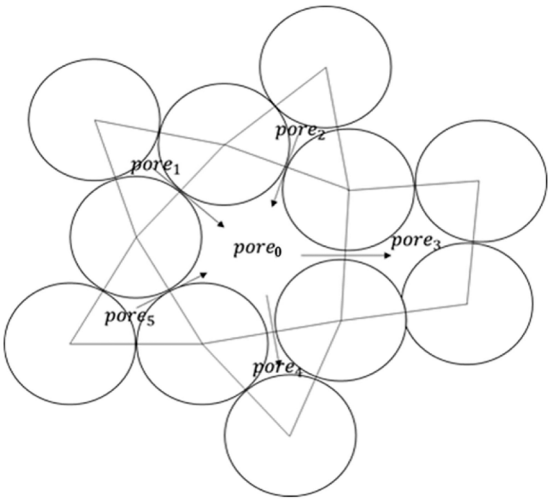

Fig. 4. Fluid migration diagram.

$$M' = M_0 + \sum_{j=1}^{n} Q_{ij}\rho_{ij} \tag{11}$$

where M_0 is the original mass of the central fluid domain, Q_{ij} is the seepage flow of each fluid domain to the central fluid domain, and ρ_{ij} is the fluid density of the outflow domain. By this method, the mass of all fluid domains in one time step can be calculated, and then the density of all fluid domains is obtained. In the two-dimensional model, the volume can be considered equal to the area of pores. After the new density and temperature (Eq. (14)) are introduced into the fluid state equation (Eq. (7)), a new pressure field distribution is obtained. The change in pressure difference causes the next step of seepage change and then forms an iterative loop of solving density, temperature and pressure. The process of fluid flow is realized through the above directions.

3.4. Hydrothermal coupling model

DEM-PNM seldom considers the effect of temperature on fluid transport. We introduce the variable temperature T into the fluid state equation, which realizes the iterative calculation of temperature, density and pressure. Generally, there are three categories of thermal exchange: thermal convection, thermal conduction, and thermal radiation. Thermal exchange in saturated porous media mainly involves thermal convection and thermal conduction (Kačur et al., 2017). The main reason of thermal convection is that the migration of fluids at different temperatures causes the changes in the temperature of pores. Thermal conduction mainly occurs between adjacent fluid domains, and the thermal conduction is spontaneously transferred from the fluid domain with high temperature to the fluid domain with low temperature.

In this model, heat is stored in the fluid and thermal convection occurs during fluid flow. Due to the interpore pressure gradients, fluid with a specified temperature flows between the pores. For a single pore (taking $pore_0$ in Fig. 4 as an example), the changed temperature $\Delta T_{\text{convection}}$ of the pore due to thermal convection is:

$$\Delta T_{\text{convect}} = \frac{\sum_{i=1}^{n} Q_i\rho_i(T_i - T_0)}{M_0 + \sum_{i=1}^{n} Q_i\rho_i} \tag{12}$$

where T_i and ρ_i are the temperature and density of the surrounding fluid domains.Q_{ij} is the seepage flow of each fluid domain to the central fluid domain. T_0 and M_0 are the initial temperature and mass of the surrounding fluid domains. The propagation direction of thermal convection is consistent with the pressure gradient. The efficiency of thermal convection is related to the pressure difference between adjacent pores. When the pressure difference is greater, the fluid velocity is faster, and the speed of thermal convection is faster.

Thermal conduction occurs between two adjacent fluid domains with different temperatures and is calculated according to the classical Fourier law. The changed temperature $\Delta T_{\text{conduct}}$ of the pore per unit time due to thermal conduction is:

$$\Delta T_{\text{conduct}} = -\frac{\phi\sum_{j=1}^{n}\frac{dT_{ij}}{l_{ij}}A_{ij}}{cM_0} \tag{13}$$

where c and M_0 are the specific heat capacity and mass of the fluid domains, ϕ is the thermal conductivity, dT_{ij}/l_{ij} is the temperature gradient between adjacent pores, and A_{ij} is the area of the pore throat. The direction of thermal conduction has nothing to do with the pressure gradient and is consistent with the direction of the temperature gradient. The efficiency of thermal conduction increases with increasing temperature gradient.

The temperature T' of the fluid domain after heat exchange after a time step is:

$$T' = T_0 + \Delta T_{\text{convect}} + \Delta T_{\text{conduct}} \tag{14}$$

where T_0 is the original temperature, $\Delta T_{convect}$ is the temperature change caused by the pressure gradient, and $\Delta T_{conduct}$ is the temperature change caused by the temperature gradient. Considering the effects of thermal convection and conduction between fluid media, the description and simulation of the complex hydrothermal coupling process is realized through the iterative calculation of the above formula. Further, the method can be used to study the simulation of solute transport, which includes the convection and diffusion phenomena.

3.5. Fluid-solid coupling model

In this model, there is a two-way coupling between fluids and solids. Elements are displaced under the action of fluid pressure difference, which causes changes in parameters such as pore volume, pore throat channel area, and local permeability coefficient. These changes can further affect the state and transport of the fluid. The fluid–solid coupling includes three steps: the action of the fluid on the solid, the action of the solid on the fluid, and the re-division of the pore network.

3.5.1. The search algorithm of pore network

The search algorithm of pore network in this paper is based on matrix calculation. Fig. 5a is the discrete element packing model composed of elements numbered 1 ~ 7. The pore network model is established based on the proposed pore throat identification method in section 3.1. Fig. 5b is the connection index matrix C based on the pore structure in Fig. 5a. The data in the first column is the index of connections, the second and third column are the serial number of starting and ending elements. Pore throats between elements are defined as connections and represented as vectors (such as (a, b), where a is the number of the starting element, and b is the number of the ending element). In the connection index matrix ***C***, connections with different starting elements are arranged in ascending order of the starting element and connections with the same starting element are arranged in ascending order of the angle θ between the vector and the positive direction of the X axis (see Fig. 5b for details). In this algorithm, connection (b, a) is defined as the anti-connection of connection (a, b). Fig. 5c is the anti-connection index matrix ***CI*** based on the connection index matrix ***C***, which makes the numbers in the second column smaller than the numbers in the third column. Therefore, connections with equal row vectors in CI are anti-connections of each other (such as connection with index 1 and connection with index 6).

As shown in Fig. 5a, (1, 2), (2, 3) and (3, 1) together constitute a pore. The connection (2, 3) is defined as the next-connection of connection (1, 2). The basic method to find the pore is to start from the initial connection and find all the next-connections that make up the pore along the fixed direction. From Fig. 5b, we can know that the difference between the index of the anti-connection and the index of the next connection is 1, so the next connections can be quickly searched based on ***C*** and ***CI***. For example, we search for the pore formed by red arrows in Fig. 5a, whose initial connection is (1, 2). First, we know that the index of the anti-connection of the initial connection is 1 based on CI. Then, the index of the next-connection can be obtained by subtracting 1 from the index of the anti-connection. Repeating this, we will eventually go back to the initial connection and get the indexes of all the connections that make up the pore: 1, 5, 9. Based on this method, we perform pore search on all connections and delete pores with the same composition, and finally the composition of all pores is obtained. We call this method simplex closed-loop search. The simplex closed-loop search will be performed in each time step, which effectively improves the computational efficiency compared with the traditional method.

3.5.2. The effect of solids on fluids

As shown in Fig. 6, for a discrete unit B_0, there are 4 pores P1 ~ P4 around it. The resultant force of the fluid on the element $(\boldsymbol{F}_f)$ can be obtained by calculating the pressure of the surrounding pores. In conventional discrete element calculations $\boldsymbol{F}_f$ is incorporated into the element force calculation, which can obtain the velocity $\boldsymbol{v}$ and displacement × of elements. After elements moved, the new volume of each pore needs to be recalculated. For example, when the fluid pressure in the pore P1 ~ P3 is high, the resultant force of the fluid on the element B_0 pushes the element B_0 to the lower left (see Fig. 6a). The effect of fluid on solid is realized based on this method.

3.5.3. The effect of solids on fluids

The effect of solids on pore seepage is reflected in the displacement of particles caused by stress which further influences the pressure and migration of fluids. The effect of the fluids on the solids can be obtained by the weighted summation of the fluid pressure and the action area vector:

$$\overrightarrow{\boldsymbol{F}_f} = \sum P_i \overrightarrow{\boldsymbol{S}_i} \tag{15}$$

During fluid seepage, changes in the pore network caused by particle displacement can further change the density and pressure of the fluid. This effect of solids on seepage can be represented by the equation of state of the fluid.The variation of stress can also cause the displacement of discrete elements, which changes the size of the pore throats and thus changes the permeability. For example, in Fig. 6b, when element B_0 is moved slightly to the lower left corner, the volume of the P4 pores

a

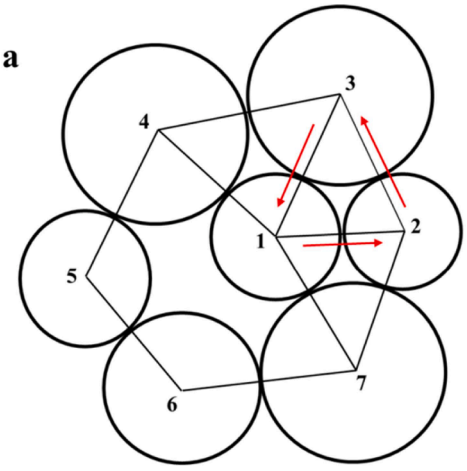

b

Index	Starting Element	Ending Element
1	1	2
2	1	3
3	1	4
4	1	7
5	2	3
6	2	1
7	2	7
8	3	4
9	3	1
10	3	2
11	4	3
12	4	5
13	4	1
14	5	4
15	5	6
16	6	7
17	6	5
18	7	2
19	7	1
20	7	6

c

Index	Starting Element	Ending Element
1	1	2
2	1	3
3	1	4
4	1	7
5	2	3
6	1	2
7	2	7
8	3	4
9	1	3
10	2	3
11	3	4
12	4	5
13	1	4
14	4	5
15	5	6
16	6	7
17	5	6
18	2	7
19	1	7
20	6	7

Fig. 5. (a)The pores in the figure are composed of elements numbered 1 ~ 7, and different elements constitute different connections; (b) The connection index matrix ***C***; (c) The anti-connection index matrix ***CI***.

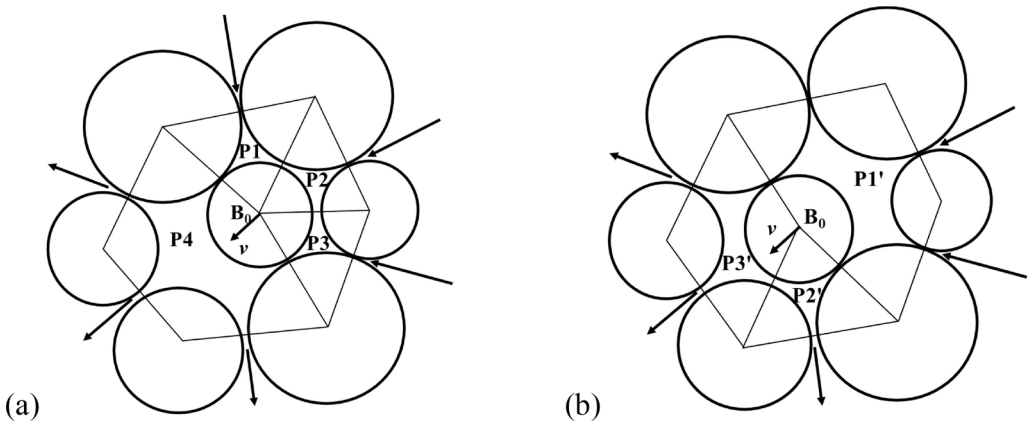

Fig. 6. (a) The initial state of the pore network. The arrow indicates the seepage direction, and the central element displaces under the action of pressure; (b) Distribution of the pore network after displacement of the central element.

decreases, which causes an increase in the density and pressure of the fluid. Correspondingly, the pressure of the fluid in pore P1 ~ P3 decreases. The effect of solid on fluid is realized based on this method.

3.5.4. Re-division of the pore network

Through simplex closed-loop search, the pore network will be re-divided before each iteration. As shown in Fig. 6a, the fluid pressure changes with seepage, which causes the displacement of the central element to displace. The displacement of the central element destroys the steady state of the pore network. As shown in Fig. 6b, after the central element is displaced, the pore network needs to be divided due to the change in the distance between the elements. The original pore network is divided and merged due to the disappearance of some old pore throats and the emergence of new pore throats. When a pore is divided, the density and pressure of these sub pores remain unchanged, and their mass is calculated according to the pore volume. When some pores are merged, the density of the new pore ρ' is the weighted sum of the density of the original pores. The dynamic division of the network is realized based on this method. Pore P4 in Fig. 6a is divided into pores P2′ and P3′ in Fig. 6b, and pore P1 ~ P3 is merged into pore P1′.

4. Verification Examples

4.1. Development Platform and Calculation process

The pore density flow model proposed in this paper is developed based on the high-performance DEM software MatDEM, which can be downloaded from *https://matdem.com*. Based on the innovative matrix discrete element computing method, it implements an efficient discrete element numerical simulation of millions of elements. At present, MATDEM has been widely used in geological engineering fields such as landslides, tunnel excavation, seismic signal inversion and geotechnical testing (Chen and Song, 2021; Xue et al., 2021; Luo et al., 2021).

Based on the theoretical model in Section 3, after establishing the model, the properties of the fluid domain (pressure, temperature) are first set, and then the initial fluid domain properties—volume, density, and mass—are systematically calculated. Driven by the internal pressure difference, fluids begin to migrate in the pore network. The density, temperature and pressure of each fluid domain after the first time step are calculated by equations. Then the pore network will be updated according to the displacement of elements. The density, temperature and pressure calculated after the first-time step will become the initial properties of the second time step. Iterating in this way can realize the numerical simulation of fluid–solid coupling. The specific process is shown in the flow chart below (Fig. 7).

Next, in this section, the discrete element model is established according to the developed code. The validation and convergence of the pore density flow model will be verified through a testing seepage experiment, a geothermal model tank experiment and a hydraulic fracturing experiment.

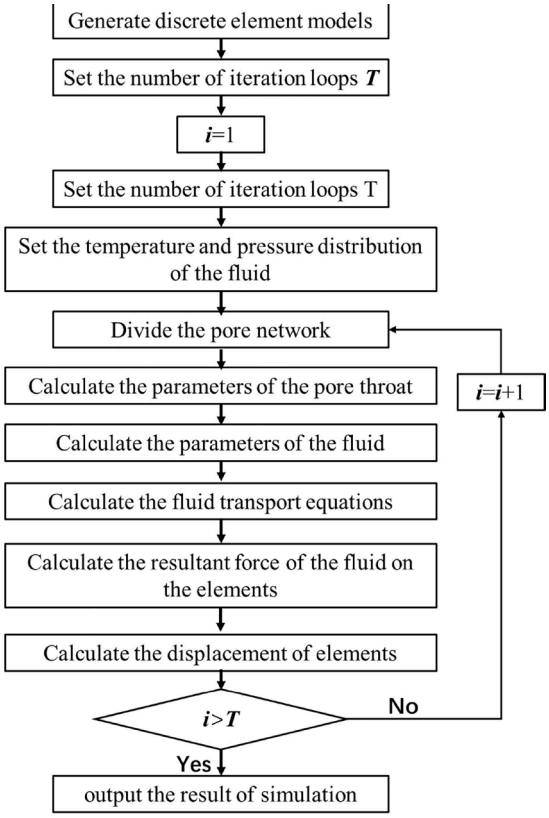

Fig. 7. Discrete element calculation flow chart.

4.2. Application example of the seepage model

We designed a discrete element model similar to the permeability meter to validate the seepage function, which can be used to measure the macro permeability coefficient and thermal conductivity of the model. Fig. 8a is the parameter calibration model we designed, the middle part is the rock and soil model we need to test, and the upper and lower voids are defined as pores, which are set as fluid boundaries during the simulation. By setting the micro permeability and thermal conductivity of the pore throats, the model has the ability of seepage and

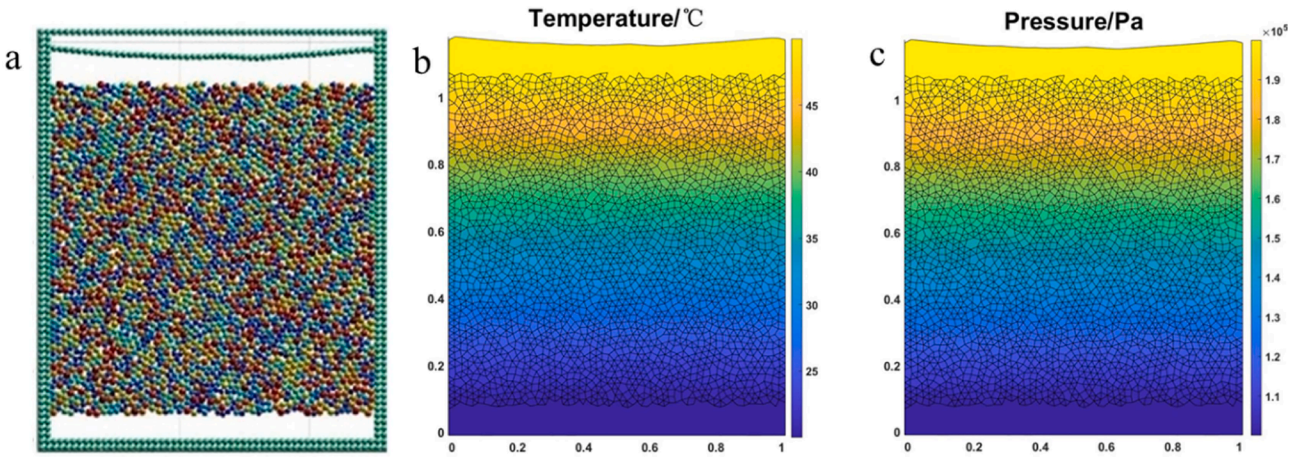

Fig. 8. (a) Initial model; (b) schematic diagram of the temperature distribution; (c) schematic diagram of the pressure distribution.

heat transfer. Ignoring the gravitational head, the upper boundary of the model is given a constant high pressure and temperature. The lower boundary is given a constant low pressure and temperature, which are consistent with the initial model. Seepage will start under the action of the vertical downward pressure field. In order to quickly obtain the permeability coefficient of the model, the coordinates of elements in this simulation are locked (only in this simulation). In this simulation, only the migration of fluid is calculated and the solid–fluid coupling is not calculated. Fig. 8b and Fig. 8c show the temperature and pressure distribution when the seepage is stable. Four points (H = 0.3 m, 0.5 m, 0.7 m, and 0.9 m) are chosen at different depths in the middle of the model to observe the pressure and temperature changes. As shown in Fig. 9a and Fig. 9b, the distribution of temperature and pressure after equilibrium are consistent with the theory, and the gradient of pressure and temperature gradient at different depths are consistent.

Fig. 10 shows the flow rates of the upper and lower boundaries. Under the action of the pressure field, the upper boundary velocity refers to the flow rate of the top pore with constant high pressure flowing into the soil per unit time. The lower boundary flow velocity refers to the flow rate of soil received by the bottom pores with constant low pressure per unit time. The migration of pressure and temperature need cost time because of the characteristics of the iterative calculation of discrete elements. After a short delay, the pressure state at the bottom will change. With the redistribution of the internal pressure of the model, the flow rate of the upper boundary decreases rapidly and is equal to that of the lower boundary, which indicates that the seepage is stable. After the seepage is stable, the macro permeability coefficient of the model can be obtained according to Darcy's law. The calibration of the heat transfer parameters is similar to that of the permeability coefficient.

In order to make the macroscopic permeability coefficient of the model equal to that of the real rock and soil mass, we need to enlarge or reduce the microscopic permeability coefficient of the pore throat. The ratio of the actual permeability coefficient to that of the model is *r* (permeability coefficient ratio). We multiply the micro permeability coefficient of the pore throat by *r* to make the permeability coefficient of the model consistent with the actual value. In this way, we have preliminarily solved the macro–micro conversion of the permeability coefficient.

4.3. Application example of the hydrothermal coupling model

The heat transfer of groundwater is of great significance for studying the distribution of geothermal fields and the transformation of surface energy (Fang et al., 2017; Zhou et al., 2022). This phenomenon can be better understood through numerical simulation of hydrothermal transport in porous media. The numerical simulation of geothermal fields is a typical hydrothermal coupling problem. Therefore, based on the geothermal model tank experiment, a discrete element model of hydrothermal coupling is established to verify the validation of the pore density flow model in hydrothermal coupling. The main body of this geothermal tank experiment is a sealed geothermal tank and a constant temperature water supply system (Fig. 11a). Water outlets and water inlets of the upper and lower aquifers are set on the top and bottom of the experimental geothermal tank. Fig. 11b is the top view of the arrangement of various temperature sensors. These sensors are inserted into the soil in the order of the top view, which can measure the

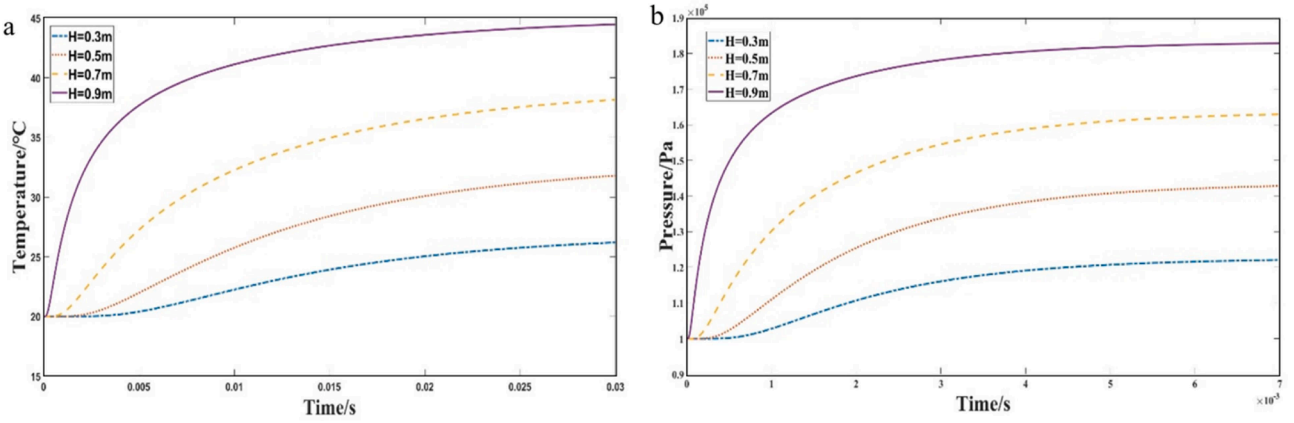

Fig. 9. (a) Changes in temperature at different depths; (b) changes in pressure at different depths.

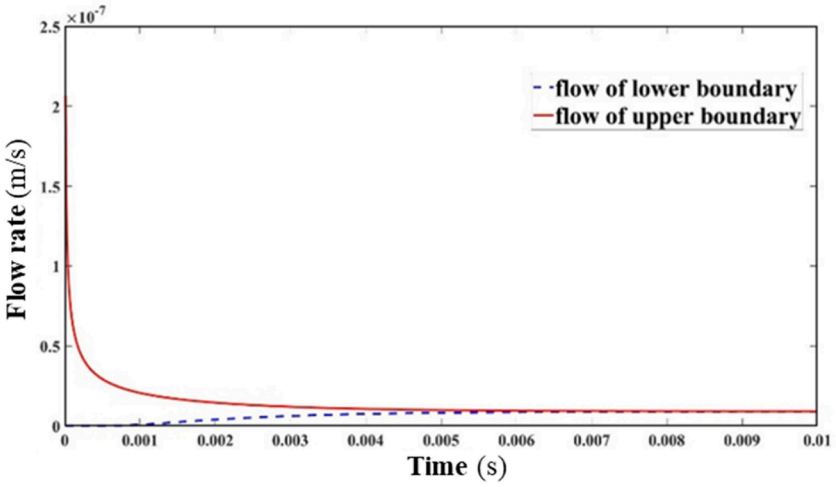

Fig. 10. Seepage volume at the upper and lower boundaries.

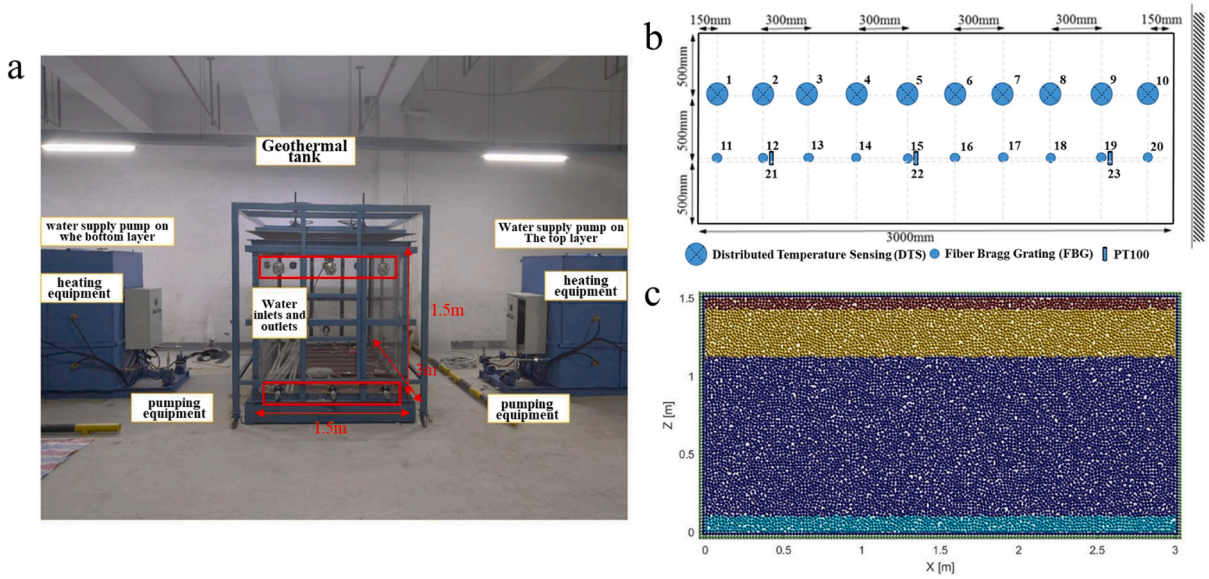

Fig. 11. (a) Geothermal tank experiment equipment; (b) Top view of the sensor arrangement; (c) Discrete Element Model of Experiments (Different colors represent soil layers with different material properties and thicknesses).

temperature at different depths in the soil. DTS is the abbreviation of Distributed Temperature Sensing and FBG is the abbreviation of Fiber Bragg Grating. They all belong to the fiber optic sensor. PT100 is a temperature sensor packaged with platinum resistance PT100 element. DTS can measure temperature at all locations along the fiber but the spatial resolution of a single fiber is not high. Therefore, the fiber in this experiment is tightly and uniformly wound on a rod equal to the height of the soil to improve the spatial resolution.

In this experiment, the soil is divided into four layers according to the material properties. From bottom to top are layer1, layer2, layer3 and layer4. Layer1 consists of breccia with a height of 100 mm. Layer2 consists of sand and kaolin in a 9:1 ratio with a height of 1015 mm. Layer 3 consists of sand and kaolin in a ratio of 8.5:1.5 with a height of 255 mm. Layer4 consists of breccia with a height of 100 mm. The permeability of the bottom layer and the top layer is the highest, and the permeability of the third layer is the lowest. As shown in Fig. 11c, the discrete element model established according to the experiment is 3 m wide and 1.5 m high. The average particle size of the elements in the model is 0.04 m. Different colors represent these soil layers with different material properties and thicknesses.

The main content of this experiment is to test the effect of the flow of groundwater at a lower temperature on the distribution of the geothermal field. First, the initial temperature inside the tank was set to 9 °C by using water outlets and water inlets. Then, the water outlets and water inlets were turned off on the top layer, and cold water was flowed at 3 °C in the bottom layer. In this discrete element model, the temperature of the fluid in the tank is set to 9 °C. The pore fluid domain in the lower left corner is given constant high pressure and constant low temperature (3 °C) to simulate groundwater inflow. The pore fluid domain in the lower right corner is given constant low pressure and high temperature (9 °C) to simulate groundwater outflow. The constant high pressure is set to 10 times the initial water pressure, and the constant low pressure is the same as the initial water pressure. The numerical simulation results are shown in Fig. 12. The pressure field enforces seepage mainly along the bottom layer, which causes a rapid decrease in the temperature of the bottom layer. The low temperature spreads slowly to the upper layer.

DTS2, DTS5, and DTS9 are selected to study the change in temperature at different sections with time (the specific locations are shown in Fig. 11b). Fig. 13a is the temperature cloud diagram obtained by the

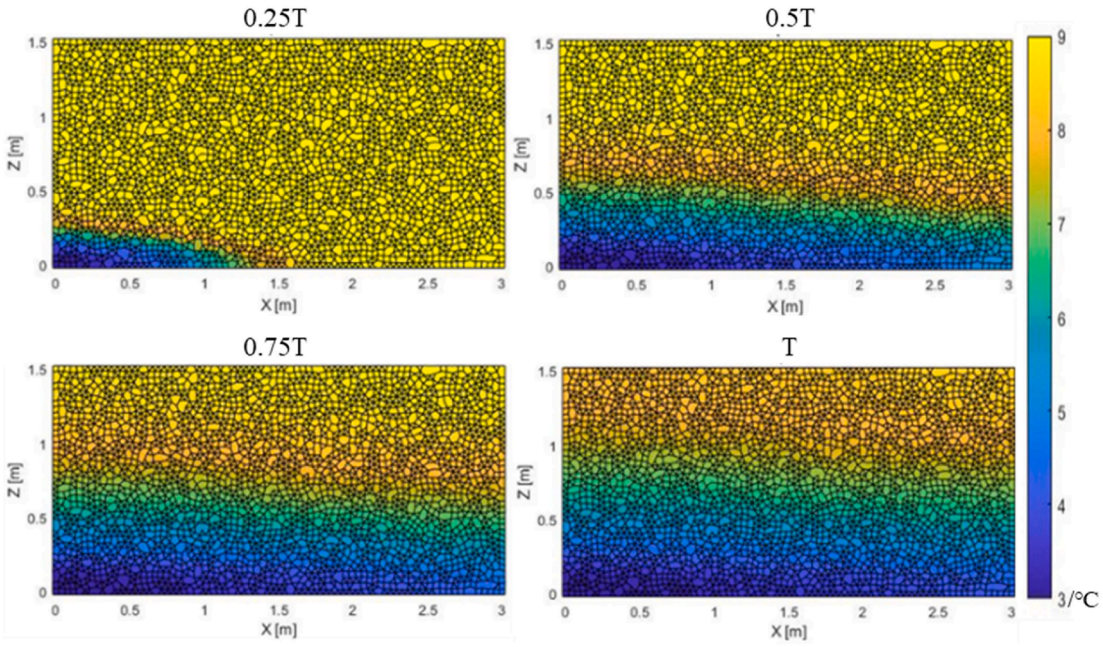

Fig. 12. The temperature field distribution of pores at different time in the simulation (0.25 T, 0.5 T, 0.75 T and T).

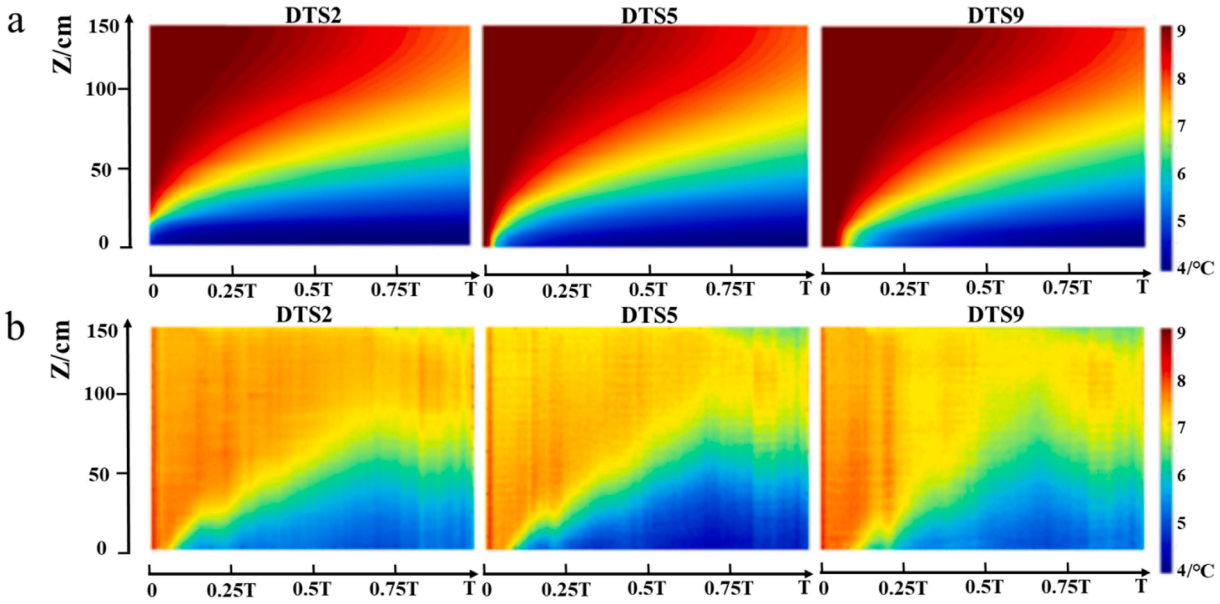

Fig. 13. Temperature-time cloud diagrams (The temperature sensors DTS2, 5, and 9 are located on the left, middle and right of the tank, respectively, and the distance from the left side of the tank is 0.45 m, 1.35 m and 2.55 m) (a) simulated by MATDEM; (b) measured by DTS.

simulation. Fig. 13b is the temperature cloud diagram monitored by the DTS. The X-axis represents time, and the Y-axis represents soil depth. Colors represent temperature values. As shown in Fig. 13, it can be seen that there is a short delay in the temperature change at the beginning, which is caused by the different positions of the sensors. The temperature of the bottom layer drops rapidly to 3 °C under the action of seepage and the temperature of the upper layers increases slowly. It can be seen that the temperature spread further in experiments than in DEM. The reason for this phenomenon is that the experimental tank cannot be completely insulated. Since the experiments lasted for a long time in winter, the heat in the experimental tank diffused outward, which led to the decrease of temperature in experiments. However, the simulations were carried out in an adiabatic environment, which caused the temperature to spread farther in DEM than in experiments. In general, the simulation results correspond well with the experimental results, which shows the influence of on the distribution of ground temperature. This simulation verifies the feasibility of the hydrothermal coupling and lays a foundation for future multi-field coupling research.

4.4. Application example of the fluid–solid coupling model

Rock hydraulic fracturing involves a complex fluid–solid coupling process. The propagation law of hydraulic fractures and the coupling mechanism between fracturing fluid and rock mass are current research hotspots and difficulties (Zhang et al., 2022). Zhang proposed a novel Galerkin-based numerical approach named global cracking elements method (GCEM) for studying the quasi-brittle fracture and the direction of crack propagation (Zhang and Zhuang, 2018; Zhang and Mang,

2020). To validate the fluid–solid coupling model, we simulate the hydraulic fracturing to compare with real experimental results. According to various physical and mechanical parameters of the hydraulic fracturing test, the hydraulic fracturing model of single fracture granite is established. The *meso*-parameters of the model were calibrated by MatDEM.

The average diameter of the elements is set to 1 mm, and the dispersion coefficient is set to 0.25. The element diameter is normally distributed between 0.80 mm and 1.24 mm. As shown in Fig. 14a, the model has a width of 75 mm and a height of 150 mm, which contains 13,437 elements. Then, the elements that make up the model will be given specific mechanical properties. According to the macro-mechanical properties of granite and the conversion formula of DEM (Liu et al., 2017), the micromechanical parameters of the elements can be obtained. The macro- and micro-mechanical parameters of the material are shown in Table 1.

Finally, precast cracks with a length of 20 mm can be obtained by deleting elements (Fig. 14b). A pressure of 20 MPa is applied to the top of the granite samples to simulate the axial pressure applied in the real world. Different water pressures are applied in the central area of the hydraulic fracture to simulate the hydraulic fracturing process until the sample breaks. The time step set by the simulation is 8×10^{-8} s, 1000 iterations per cycle. The simulated object is selected as the prefabricated fracture sample, which forms an angle of 30°, 60° and 90° with the horizontal plane. The initial state of the model is shown in Fig. 14b.

By comparing the experimental results with the simulation results (as shown in Fig. 15), it can be seen that the crack develops from both ends in the direction of maximum principal stress. At the same time, we can see that the experimental results (90°) are not completely developed strictly along the direction of the maximum principal stress. There are some micro-cracks in the real rock, which make the mechanical structure of the rock have a certain anisotropy, and make the extension direction of the cracks deflect to a certain extent. However, there are no micro-cracks in the simulated rock, and the overall mechanical properties are isotropic, so the simulated cracks develop along the direction of the maximum principal stress. In general, the simulation process and results are consistent with the experiment, verifying the feasibility of applying the fluid–solid coupling model to hydraulic fracturing. In addition, the development of fractures driven by fluid and the redivision of networks during large deformation are also validated.

5. Discussion and conclusions

In this paper, a pore density flow model is constructed based on the Discrete Element Method (DEM) and the Pore Network Model (PNM) and we can apply it in various fields. The Pore Network Model is adopted

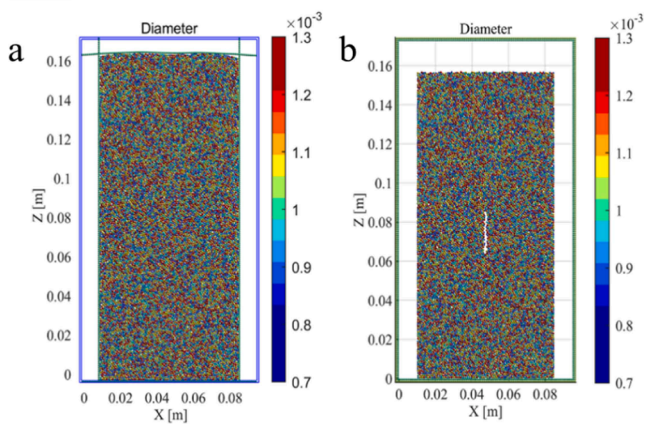

Fig. 14. The discrete element model (a) The initial stacking model; (b) The elements in the middle of the model are removed to form precast cracks (90°).

Table 1
Macro- and micro-mechanical parameters of materials.

Macroscopic mechanical parameters		**Micromechanical parameters**	
Mechanical parameters	Test value	Mechanical parameters	Average value
Young's modulus E/GPa	77.10	Normal stiffness K_n/(N·m^{-1})	2.57×10^7
Poisson's ratio ν	0.18	Tangential stiffness K_s/(N·m^{-1})	3.14×10^6
tensile strength Tu/MPa	6.49	Fracture displacement X_b/m	1.40×10^{-6}
Compressive strength Cu/MPa	128	Shear resistance F_{s0}/N	94.3
Coefficient of internal friction μ_i	1	Coefficient of friction μ_p	2.0

to the calculation of the fluid for exerting its advantages in solving seepage in porous media. The structure and parameters of the pore network are controlled by the structure of discrete elements. In the seepage calculation based on Darcy's law, the fluid state equation containing temperature parameters and heat exchange equation are introduced to ensure the correctness of the hydrothermal coupling model. The Discrete Element Method is adopted to track the behavior of solid particles. In this model, the structural changes of the pore network is well considered during the deformation and destruction of the discrete element model. Compared with the conventional model, the model in this paper can simulate the fluid-driven fracturing for complex fractured porous media, which can simulate the intersection and development of arbitrarily complex fractures. This model is implemented in the high-performance discrete element software MatDEM. Both the redivision of pore network and the calculation of particle motion use matrix calculation, which is highly efficient, especially for large-scale calculations.

To demonstrate the capability and applicability of the proposed model in multi-field coupled and fluid–solid coupled applications, three numerical simulations were performed. The seepage simulation demonstrated the validity of the pore network and the seepage model. In the simulation of the geothermal model tank experiment, the immigration of fluids and heat can be accurately captured, which proves the feasibility of the hydrothermal coupling model. The simulations of hydraulic fracturing experiment emphasize the importance of two-way coupling. The development of fractures driven by fluid is captured in this simulation, which demonstrates the applicability of fluid–solid coupling and the importance of bidirectional coupling. The results of the simulation are in good agreement with those of the corresponding experiment.

In the considered numerical simulations, the potential and applicability of the pore density flow model is demonstrated, albeit within a limited range (i.e. single-phase seepage in porous saturated media). However, this model can be combined with multiphase flow theory, liquid bridge model and other theories to build multiphase saturated/unsaturated models to solve the complex multi-field coupling and fluid–solid coupling problems in geotechnical engineering. First, through the phase expansion of the fluid state equation, the state of the fluid changes from single phase to multiphase, which can be used to simulate magma intrusion and freeze–thaw effects. Then, by combining the solute transport equation with the seepage model, more complex multi-field coupled phenomena can be simulated. Finally, by simulating the seepage of unsaturated fluids and determining the forces between particles based on the liquid bridge model, the formation mechanism of rainfall landslides can be explored. These works need to be further developed so that the proposed numerical model can be more deeply used in the simulation of multi-field coupling and fluid–solid coupling.

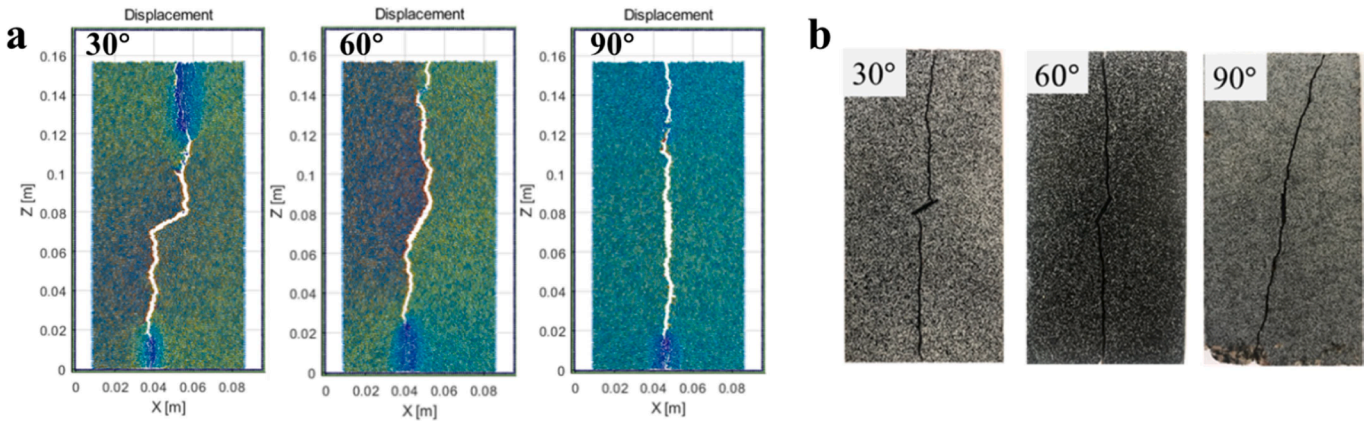

Fig. 15. (a) The development of cracks in the numerical simulations; (b) The development of cracks in the experiments.

CRediT authorship contribution statement

Yao Zhu: Conceptualization, Methodology, Software, Investigation, Formal analysis, Writing – original draft. **Chun Liu:** Conceptualization, Funding acquisition, Resources, Supervision, Writing – review & editing. **Hui Liu:** Software, Visualization, Investigation. **Yu-dong Kou:** Formal analysis. **Bin Shi:** Funding acquisition.

Declaration of Competing Interest

The authors declare that they have no known competing financial interests or personal relationships that could have appeared to influence the work reported in this paper.

Data availability

Data will be made available on request.

Acknowledgements

This work was supported by the National Natural Science Foundation of China (41977218, 42222707), State Key Laboratory for Geo-Mechanics and Deep Underground Engineering, China University of Mining & Technology (SKLGDUEK2117) and the Fundamental Research Funds for the Central Universities (14380103).

References

Catalano, E., Chareyre, B., Barthélémy, E., 2013. Pore-scale modeling of fluid-particles coupling and emerging poromechanical effects. Int. J. Num. Anal. Methods Geomech. 38.
Chen, Z., Song, D., 2021. Numerical investigation of the recent Chenhecun landslide (Gansu, China) using the discrete element method. Nat. Hazards: J. Int. Soc. Prevent. Mitigation Nat. Hazards 105.
Cundall, P.A., Strack, O., 1979. A discrete numerical model for granual assemblies. Geotechnique 29 (1), 47–65.
Fang, Y., Zhan, W., Huang, F., Lun, G., Zou, Z., Quan, J., 2017. Hourly variation of surface urban heat island over the yangtze river delta urban agglomeration. Adv. Earth Sci. 32 (2).
Fatt, I., 1956. The network model of porous media. Trans. AIME 207 (1).
Han, Y., Cundall, P.A., 2013. LBM–DEM modeling of fluid–solid coupling in porous media. Int. J. Numer. Anal. Meth. Geomech. 37 (10).
Huang, J., Xiao, F., Labra, C., Sun, J., Yin, X., 2021. DEM-LBM simulation of stress-dependent absolute and relative permeabilities in porous media. Chem. Eng. Sci. 239 (2), 116633.
Huang, M., Jia, C.Q., 2009. Strength reduction fem in stability analysis of soil slopes subjected to transient unsaturated seepage. Comput. Geotech. 36 (1–2), 93–101.
Indraratna, B., Phan, N.M., Nguyen, T.T., Huang, J., 2021. Simulating Subgrade Soil Fluidization Using LBM-DEM Coupling. Int. J. Geomech. 21 (5), 04021039.
Jiang, M.J., Zhang, F.G., Sun, Y.G., Zhang, W.C., 2012. DEM simulation of mechanical behaviour and bond breakage of different cemented sands. Yantu Gongcheng Xuebao/Chinese J. Geotech. Eng. 34 (11), 1969–1976.
Kačur, J., Mihala, P., Tóth, M., 2017. Heat exchange and unsaturated-saturated flow in porous media. Defect Diffusion Forum 380, 107–114.
Kharaghani, A., Metzger, T., Tsotsas, E., 2011. A proposal for discrete modeling of mechanical effects during drying, combining pore networks with DEM. AIChE J. 57.
Kuhn, M.R., Daouadji, A., 2020. Simulation of undrained quasi-saturated soil with pore pressure measurements using a discrete element (DEM) algorithm. Soils Found. 60 (5), 1097–1111.
Liu, C., Le, T.C., Shi, B., Zhu, Y., 2020. Discussion on three major problems of engineering application of the element discrete element method. Chinese J. Rock Mech. Eng. 39 (06), 1142–1152.
Liu, C., Pollard, D.D., Gu, K., Shi, B., 2015. Mechanism of formation of wiggly compaction bands in porous sandstone: 2. Numerical simulation using discrete element method. J. Geophys. Res. Solid Earth 120 (12), 8153–8168.
Liu, C., Pollard, D.D., Shi, B., 2013. Analytical solutions and numerical tests of elastic and failure behaviors of close-packed lattice for brittle rocks and crystals. J. Geophys. Res. Solid Earth 118 (1), 71–82.
Liu, C., Xu, Q., Shi, B., Deng, S., Zhu, H., 2017. Mechanical properties and energy conversion of 3D close-packed lattice model for brittle rocks. Comput. Geosci. 103 (JUN.), 12–20.
Long, J., Li, C., Liu, Y., Feng, P., Zuo, Q., 2022. A multi-feature fusion transfer learning method for displacement prediction of rainfall reservoir-induced landslide with step-like deformation characteristics. Eng. Geol. 297, 106494-.
Lu, C.Y., Tang, C.L., Chan, Y.C., Hu, J.C., Chi, C.C., 2014. Forecasting landslide hazard by the 3d discrete element method: a case study of the unstable slope in the lushan hot spring district, central taiwan. Eng. Geol. 183, 14–30.
Luo, H., Xing, A., Jin, K., Xu, S., Zhuang, Y., 2021. Discrete element modeling of the Nayong rock avalanche, Guizhou, China constrained by dynamic parameters from seismic signal inversion. Rock Mech. Rock Eng. 54 (4), 1629–1645.
Nian, T.K., Li, D.Y., Liang, Q.H., Wu, H., Guo, X.S., 2021. Multi-phase flow simulation of landslide dam formation process based on extended coupled DEM-CFD method. Comput. Geotech. 140, 104438.
Norouzi, H.R., Zarghami, R., Sotudeh-Gharebagh, R., Mostoufi, N., 2016. CFD-DEM Applications to Multiphase Flow. John Wiley & Sons Ltd.
Place, D., Mora, P., 1999. The lattice solid model to simulate the physics of rocks and earthquakes: incorporation of friction. J. Compos. Phys. 150 (2), 332–372.
Qu, D., Luo, Y., Li, X., Wang, G., Xu, K., 2020. Study on the stability of rock slope under the coupling of stress field, seepage field, temperature field and chemical field. Arab. J. Sci. Eng. 45 (10), 8315–8329.
Rettinger, C., Rüde, U., 2018. A coupled lattice boltzmann method and discrete element method for discrete particle simulations of particulate flows. Comput. Fluids 172, 706–719.
Sizkow, S.F., El Shamy, U., 2021. SPH-DEM simulations of saturated granular soils liquefaction incorporating particles of irregular shape. Comput. Geotech. 134, 104060.
Sizkow, S.F., El Shamy, U., 2022. SPH-DEM modeling of the seismic response of shallow foundations resting on liquefiable sand. Soil Dyn. Earthq. Eng. 156, 107210.
Tsang, Y.W., Witherspoon, P.A., 1981. Hydromechanical behavior of a deformable rock fracture subject to normal stress. J. Geophys. Res. Solid Earth 19 (5), 107.
Wautier, A., Bonelli, S., Nicot, F., 2017. Scale separation between grain detachment and grain transport in granular media subjected to an internal flow. Granular Matter 19 (2).
Xu, W.J., Yao, Z.G., Luo, Y.T., Dong, X.Y., 2020. Study on landslide-induced wave disasters using a 3D coupled SPH-DEM method. Bull. Eng. Geol. Environ. 79 (1), 467–483.
Xue, Y., Zhou, J., Liu, C., Far, M.S., Zhang, J., 2021. Rock fragmentation induced by a TBM disc-cutter considering the effects of joints: a numerical simulation by DEM. Comput. Geotech. 136, 104230.
Yuan, C., Chareyre, B., Darve, F., 2016. Pore-scale simulations of drainage in granular materials: finite size effects and the representative elementary volume. Adv. Water Resour. 95, 109–124.
Zhang, J., Yu, H., Xu, W., Lv, C., Micheal, M., Shi, F., Wu, H., 2022. A hybrid numerical approach for hydraulic fracturing in a naturally fractured formation combining the XFEM and phase-field model. Eng. Fract. Mech. 108621.

Zhang, Y.M., Mang, H.A., 2020. Global cracking elements: a novel tool for Galerkin-based approaches simulating quasi-brittle fracture. Int. J. Numer. Meth. Eng. 121, 2462–2480.
Zhang, Y.M., Zhuang, X., 2018. Cracking elements: a self-propagating strong discontinuity embedded approach for quasi-brittle fracture. Finite Elements Anal. Des. 144(MAY), 84-100.
Zheng, X., Duan, W.Y., Ma, Q.W., 2010. Comparison of improved meshless interpolation schemes for SPH method and accuracy analysis. J. Mar. Sci. Appl. 9 (3), 223–230.
Zhou, X.P., Du, E.B., Wang, Y.T., 2022. Thermo-hydro-chemo-mechanical coupling peridynamic model of fractured rock mass and its application in geothermal extraction. Comput. Geotech. 148, 104837.
Zhou, Y., Chen, L., Gong, Y., Wang, S., 2021a. Pore-scale simulations of particles migration and deposition in porous media using LBM-DEM coupling method. Processes 9 (3), 465.
Zhou, Z.Q., Ranjith, P.G., Yang, W.M., Shi, S.S., Wei, C.C., Li, Z.H., 2019. A new set of scaling relationships for DEM-CFD simulations of fluid–solid coupling problems in saturated and cohesiveless granular soils. Computat. Part. Mech. 6 (4), 657–669.
Zhou, Z., Ding, H., Gao, W., Xu, L., 2021b. Study on mechanical properties of soil-rock mixture of various compactness subjected to freeze-thaw cycles. Sci. Cold Arid Regions 13 (5), 450–462.

Further reading

Jackson, R., 1997. Locally averaged equations of motion for a mixture of identical spherical particles and a Newtonian fluid. Chem. Eng. Sci. 52 (15), 2457–2469.
Jiang, M.J., 2019. New paradigm for modern soil mechanics: Geomechanics from micro to macro. Chinese J. Geotech. Eng. 41 (02), 195–254.
Yuan, C., Chareyre, B., 2017. A pore-scale method for hydromechanical coupling in deformable granular media. Comput. Methods Appl. Mech. Eng. 318 (MAY1), 1066–1079.
Zhou, Z.Y., Kuang, S.B., Chu, K.W., Yu, A.B., 2010. Discrete particle simulation of particle–fluid flow: model formulations and their applicability. J. Fluid Mech. 661, 482–510.